This is an open access article published under an ACS AuthorChoice License, which permits copying and redistribution of the article or any adaptations for non-commercial purposes.

ACS OMEGA

http://pubs.acs.org/journal/acsodf

Article

Rubidium and Cesium Enediamide Complexes Derived from Bulky 1,4-Diazadienes

Ramesh Duraisamy, Phil Liebing, Nicole Harmgarth, Volker Lorenz, Liane Hilfert, Martin Feneberg, Rüdiger Goldhahn,* Felix Engelhardt, and Frank T. Edelmann*

Cite This: *ACS Omega* 2020, 5, 19061−19069

Read Online

ACCESS | Metrics & More | Article Recommendations | Supporting Information

ABSTRACT: The first rubidium and cesium enediamide complexes based on bulky 1,4-diaza-1,3-diene ligands (DADs) have been prepared by metalation of either 1,4-bis(2,6-diisopropylphenyl)-1,4-diaza-1,3-butadiene (**1**, = $^{H2}DAD^{Dipp}$) or 1,4-bis(2,6-diisopropylphenyl)-2,3-dimethyl-1,4-diaza-1,3-butadiene (**2**, = $^{Me2}DAD^{Dipp}$) with an excess of Rb or Cs metals in coordinating solvents such as tetrahydrofuran (THF) or 1,2-dimethoxyethane (DME). All new complexes were fully characterized by spectroscopic and analytical methods as well as single-crystal X-ray diffraction studies.

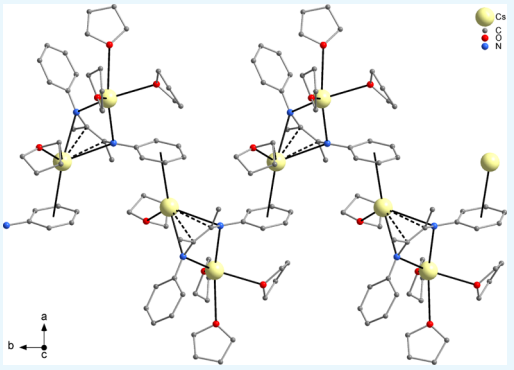

Downloaded via OTTO VON GUERICKE UNIV on April 29, 2021 at 09:18:29 (UTC).
See https://pubs.acs.org/sharingguidelines for options on how to legitimately share published articles.

INTRODUCTION

For more than five decades, DADs (1,4-diaza-1,3-dienes) of the composition R−N═C(R′)−C(R′)═NR have been employed as highly useful ligands for main group elements, transition−metals, and f-elements.[1−4] As illustrated in Scheme 1, DADs are redox noninnocent ligands which can undergo a reversible stepwise reduction to the radical anion and the enediamide dianion.

Scheme 1. Reversible Stepwise Reduction of 1,4-Diaza-1,3-dienes

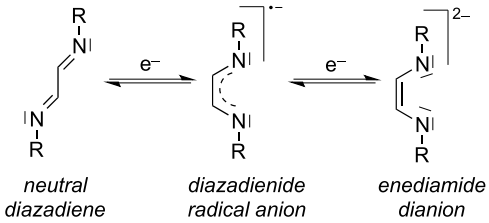

Scheme 2 illustrates the typical coordination modes found in metal DAD complexes. Mononuclear complexes can contain neutral (**A**), radical monoanionic (**B**), and dianionic enediamide-type DAD ligands (**C**) in a characteristic *κN,κN′*-chelating coordination mode. η^4-Coordination of the π-electron system is also possible in monometallic complexes. In this case, the metal atom is located above the C_2N_2 plane (*cf.* Scheme 2 **D**). Different combinations of σ- and π-coordination modes were found in dinuclear DAD complexes,

Scheme 2. Different Coordination Modes of 1,4-Diaza-1,3-dienes in Mononuclear (A−D) and Dinuclear Metal DAD Complexes (E, F)

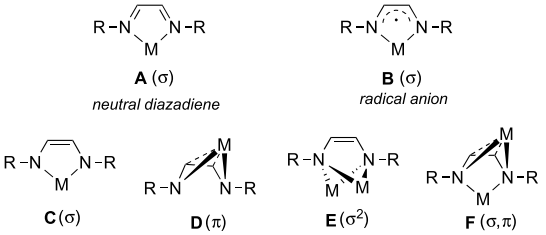

including the symmetric σ^2-coordination of the two nitrogen atoms (**E**) and a mixed σ,π-coordination mode (**F**).[1−5]

Metal DAD complexes comprising the ligand in its enediamide form are known for the lanthanide elements,[6−15] early transition-metals[16−25] and some late transition-metals.[26,27] Enediamide complexes have also found some practical applications. Recently, it was demonstrated that an Yb(III) enediamide complex behaves as a single-ion magnet,[14] whereas several group 4 metal enediamide complexes turned out to be

Received: May 22, 2020
Accepted: July 9, 2020
Published: July 23, 2020

© 2020 American Chemical Society

https://dx.doi.org/10.1021/acsomega.0c02414
ACS Omega 2020, 5, 19061−19069

useful homogeneous catalysts for the ring-opening polymerization of cyclic esters[9] and for olefin polymerization.[23]

The general synthetic route to metal enediamide complexes involves the treatment of metal halide precursors with the alkali metal derivatives of the enediamide dianions.[6,8−11,13,20,28] The preparation of the latter can be achieved by 2-electron reduction of the free DAD ligands with an excess (>2 equiv) of alkali metals (M = Li, Na, K) in coordinating solvents such as tetrahydrofuran (THF) or 1,2-dimethoxyethane (DME). This results in the formation of orange solutions of M_2DAD with can be directly used for salt-metathetical reactions with metal halides. Frequently employed DAD ligands include derivatives with sterically demanding 2,6-diisopropylphenyl (Dipp) groups at the N atoms, for example, 1,4-bis(2,6-diisopropylphenyl)-1,4-diaza-1,3-butadiene (**1**, = ^{H2}DAD^{Dipp}) and 1,4-bis(2,6-diisopropylphenyl)-2,3-dimethyl-1,4-diaza-1,3-butadiene (**2**, = ^{Me2}DAD^{Dipp}) (Scheme 3). These ligands can be easily prepared by the reaction of glyoxal or diacetyl with 2 equiv of 2,6-diisopropylaniline and isolated in the form of bright yellow crystalline solids.[29,30]

Scheme 3. Representation of the Sterically Demanding Ligands ^{H2}DAD^{Dipp} (1) and ^{Me2}DAD^{Dipp} (2)

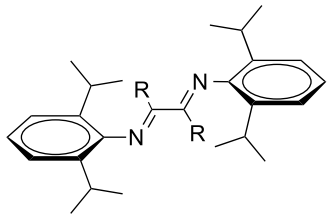

1: R = H (^{H2}DAD^{Dipp})
2: R = Me (^{Me2}DAD^{Dipp})

Several alkali metal enediamide complexes containing **1** and **2** have already been described in the previous literature, but these are limited to Li, Na, and K thus far. In a recent contribution, we have shown that the molecular structures of these compounds are predominantly governed by the substituents at the DAD ligand and less by the choice of metal.[31] In the complexes of all three metals Li, Na, and K, the ligand $(^{H2}DAD^{Dipp})^{2-}$ displays a more or less symmetric σ^2-coordination to the two metal center (*cf.* type **E** in Scheme 1), while a mixed σ,π-coordination was always observed with the $(^{Me2}DAD^{Dipp})^{2-}$ ligand (*cf.* type **F** in Scheme 1). We have now been interested in the question if this behavior continues when going to the heaviest of the alkali metals, Rb and Cs, or if the structures of their complexes is increasingly impacted by the higher affinity of these metals to π-coordinating ligands. We report here the synthesis and full characterization of the first rubidium and cesium enediamide complexes as well as their molecular and crystal structures as determined by X-ray crystallography.

RESULTS AND DISCUSSION

Synthesis and Characterization of the Rubidium and Cesium Enediamide Complexes 3−6. As illustrated in Scheme 4, the first rubidium and cesium enediamide complexes derived from **1** and **2** were synthesized and fully characterized in the course of the present study. Similar to the previously reported Li, Na, and K reactions,[31] the stepwise reduction of **1** and **2** by the two heavy alkali metals was clearly

Scheme 4. Synthetic Route to the Title Complexes 3−6

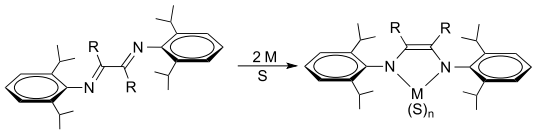

1 : R = H (^{H2}DAD^{Dipp})
2 : R = Me (^{Me2}DAD^{Dipp})

3 : R = H, M = Rb, $(S)_n$ = (THF)
4 : R = H, M = Cs, $(S)_n$ = $(DME)_2$
5 : R = Me, M = Rb, $(S)_n$ = $(THF)_4$
6 : R = Me, M = Cs, $(S)_n$ = $(THF)_4$

observed by a series of typical color changes. Stirring of solutions of **1** or **2** in THF or DME with an excess of 2 equiv (to ensure total consumption of the DAD starting materials) of rubidium or cesium first resulted in the appearance of an intense dark-red color typical for the radical-anionic species $(DAD)^{\bullet-}$. Prolonged stirring of the reaction mixtures resulted in replacement of the very dark coloration by a significantly lighter orange color, indicating the formation of the enediamide dianion DAD^{2-}. Unreacted metal was removed by filtration, and the orange filtrates were concentrated under vacuum to a small volume. The solvated products $Rb_2(^{H2}DAD^{Dipp})(THF)$ (**3**), $Cs_2(^{H2}DAD^{Dipp})(DME)_2$ (**4**), $Rb_2(^{Me2}DAD^{Dipp})(THF)_4$ (**5**), and $Cs_2(^{Me2}DAD^{Dipp})(THF)_4$ (**6**) crystallized directly at room temperature from the concentrated solutions.

All products **3−6** were isolated as deep red, plate-like or prism-like, highly air- and moisture-sensitive crystals and were fully characterized by analytical and spectroscopic methods. The mass spectra showed mainly fragment ions of the coordinated diazadiene ligands, whereas ions with higher masses appeared only with very low relative intensities. This is in accordance with the presence of highly polar alkali metal compounds. However, in contrast to the paramagnetic alkali metal derivatives of DAD radical anions,[5] the title complexes are diamagnetic, so that characterization by NMR spectroscopy was possible. The ^{1}H and ^{13}C NMR spectra in THF-d_8 solution showed typical signals of the DAD ligands and the coordinated solvents. Solubility problems were only encountered in the case of cesium derivative **4**. Once isolated in the crystalline form, this compound showed a remarkably low solubility in THF and DME, so that NMR data could only be obtained in pyridine-d_5, where the partial overlap with the solvent resonance precluded a complete assignment of all signals. Generally, all compounds showed one set of DAD ligand signals in their ^{1}H and ^{13}C NMR spectra, and the shifts resembled the values observed for the corresponding Li, Na, and K analogs.[31] As illustrated in Scheme 4, the formation of the title complexes **3−6** is accompanied by a two-electron reduction of the neutral 1,4-diazadienes to the metal-coordinated enediamide dianion. This is clearly evidenced by significant changes in the ^{1}H and ^{13}C NMR spectra of the Rb and Cs complexes in comparison the spectra of the DAD precursors **1** and **2**. Particularly informative in this respect are the signals of the central −NC(R)C(R)N− unit (R = H, CH_3). For example, the central CH resonance signal in **1** is observed at δ 8.14 ppm, whereas it appears as a broad peak at δ 5.48−5.65 ppm in the spectrum of Rb complex **3** (in the ^{1}H NMR spectrum of **4**, this signal is hidden underneath the aromatic proton signals of the Dipp moieties). Similar shifts are observed for the central CH_3 signals in the free ligand **2** (δ 2.08 ppm) versus the metal complexes **5** (δ 1.62 ppm) and **6** (δ 1.56 ppm). In the ^{13}C NMR spectra of the free ligands the signals of the central DAD carbon atoms are observed at δ

https://dx.doi.org/10.1021/acsomega.0c02414
ACS Omega 2020, 5, 19061−19069

Table 1. Crystal Data and Details on Structure Refinement for Compounds 3−6

compound	3	4	5·0.5 THF	6·THF
CCDC deposition number	1960467	1960468	1960469	1960470
molecular formula sum	$C_{30}H_{44}N_2ORb_2$	$C_{32}H_{51}Cs_2N_2O_3$	$C_{92}H_{152}N_4O_9Rb_4$	$C_{48}H_{80}Cs_2N_2O_5$
formula weight/g mol^{-1}	619.61	777.56	1800.05	1030.96
crystal system	monoclinic	triclinic	monoclinic	monoclinic
space group	$P2_1/n$	$P\bar{1}$	$P2_1/c$	$C2/c$
cell metric a/Å	13.2032(1)	11.0782(7)	36.5255(7)	39.16(2)
b/Å	17.7108(1)	13.4018(8)	12.5779(2)	12.227(4)
c/Å	13.3568(1)	13.8529(8)	21.3866(5)	21.282(7)
α/deg	90	64.885(4)	90	90
β/deg	104.055(1)	85.879(5)	105.589(2)	104.40(4)
γ/deg	90	69.433(5)	90	90
cell volume/Å^3	3029.84(4)	1736.3(2)	9463.9(3)	9870(8)
molecules per cell z	4	2	4	8
electrons per cell F_{000}	1280	782	3808	4256
calcd. density ρ/g cm^{-3}	1.358	1.487	1.263	1.388
diffractometer	Xcalibur, Atlas, Nova	STOE IPDS 2T	STOE IPDS 2T	STOE IPDS 2T
T/K	100(2)	153(2)	133(2)	100(2)
μ/mm^{-1} (radiation)	4.353 (Cu Kα)	2.131 (Mo Kα)	2.110 (Mo Kα)	1.521 (Mo Kα)
absorption correction	multi-scan[34]	numerical[35]	numerical[35]	numerical[35]
crystal shape and color	red prism	red rod	red plate	orange plate
crystal size/mm	0.12 × 0.08 × 0.04	0.35 × 0.16 × 0.14	0.45 × 0.20 × 0.14	0.17 × 0.12 × 0.07
θ range/deg	4.223−74.992	2.144−5.999	1.897−24.999	1.943−25.199
reflections collected	94,285	15,109	48,333	26,718
reflections unique	6244	6806	16,209	8878
reflections with $I > 2\sigma(I)$	5938	5688	11,844	7592
completeness of dataset	99.9%	99.7%	97.4%	99.7%
R_{int}	0.0394	0.0413	0.0720	0.0628
parameters; restraints	324; 0	401; 136[a]	1078; 210[a]	756; 2939[a]
R_1 (all data, $I > 2\sigma(I)$)	0.0247; 0.0234	0.0351; 0.0251	0.0825; 0.0517	0.0760; 0.0624
wR_2 (all data, $I > 2\sigma(I)$)	0.0599; 0.0589	0.0572; 0.0546	0.1186; 0.1060	0.1378; 0.1321
GooF (F^2)	1.027	0.990	1.036	1.211
Max. residual peaks	−0.610; 0.581	−0.683; 0.748	−0.561; 0.792	−1.240; 0.695
extinction coefficient				0.00059(4)

[a]Restraints were applied on the interatomic distances and anisotropic displacement parameters within disordered solvent molecules (THF or DME).

168.8 ppm (**1**, N=CH−) and δ 164.2 ppm (**2**, N=C(Me)−), respectively. Metal complexation and enediamide formation leads to an upfield shift of these signals by *ca.* 40 ppm (**3**: 121.8; **4**: 122.9; **5**: 121.5, **6**: 121.8 ppm). Raman spectra could be obtained for $^{H2}DAD^{Dipp}$-derived compounds **3** and **4** (see Supporting Information). The spectrum of compound **3** shows a strong and broad luminescence background peaking around 660 nm (about 3500 cm^{-1} for 532 nm laser excitation), and the spectra of both compounds are characterized by a variety of Raman lines between 400 and 1700 cm^{-1}. Dominating are lines between 1100 and 1700 cm^{-1} for compound **3** (1000 and 1600 cm^{-1} for compound **4**), whereas all lines below 1000 cm^{-1} are very faint. While a specialized theoretical description is lacking, we note that a very simple harmonic oscillator model is able to describe the shifts of some Raman signals between compounds **3** and **4**, assuming reduced masses for nitrogen and M (M = Rb, Cs). The triplet of bands at 1557, 1590, and 1647 cm^{-1} for compound **3** shifts to 1524, 1553, and 1585 cm^{-1} for compound **4**, yielding a constant frequency ratio of around 0.97. The same ratio is found for the 1047 cm^{-1} mode in compound **3** (1016 cm^{-1} in compound **4**) which is nearly equal to the square root of the reduced mass ratio. This is on the same order as the observed Raman mode shifts in RbN_3 and CsN_3[32,33] and can pave the way for microscopically identifying these bands.

Molecular and Crystal Structures of the Rubidium and Cesium Enediamide Complexes 3−6. Similar to their lighter alkali metal homologues,[31] compounds **3**−**6** display in their crystal structures well-defined M_2DAD units with the two metal atoms being attached to the central enediamide unit. Experimental details on the crystal structure determinations are summarized in Table 1. As outlined previously,[31] the geometric structure of the M_2DAD core can be described using the displacement angle δ, which can be defined as the angle between the MN_2 coordination plane and the C_2N_2 plane of the DAD ligand. A comparison of the M_2(DAD) structural cores of **3**−**6** is illustrated in Figure 1, and important geometric parameters for all alkali metal complexes are listed in Table 2.

Comparison of the M_2(DAD) structures in **3**−**6** revealed a similar picture as for the Li, Na, and K complexes, as the molecular conformation is predominantly governed by the ligand and less by the metal.[31] In compounds **3** and **4**, the $(^{H2}DAD^{Dipp})^{2-}$ ligand displays a σ^2-coordination to the two metal atoms (*cf.* structure **E** in Scheme 2). In **4**, both Cs atoms are coordinated quite symmetrically with δ values of 72.7(1) and 74.1(1)°, while the coordination is less symmetric for the Rb atoms in **3** [δ 64.2(2) and 78.2(2)°]. Generally, the

https://dx.doi.org/10.1021/acsomega.0c02414
ACS Omega 2020, 5, 19061−19069

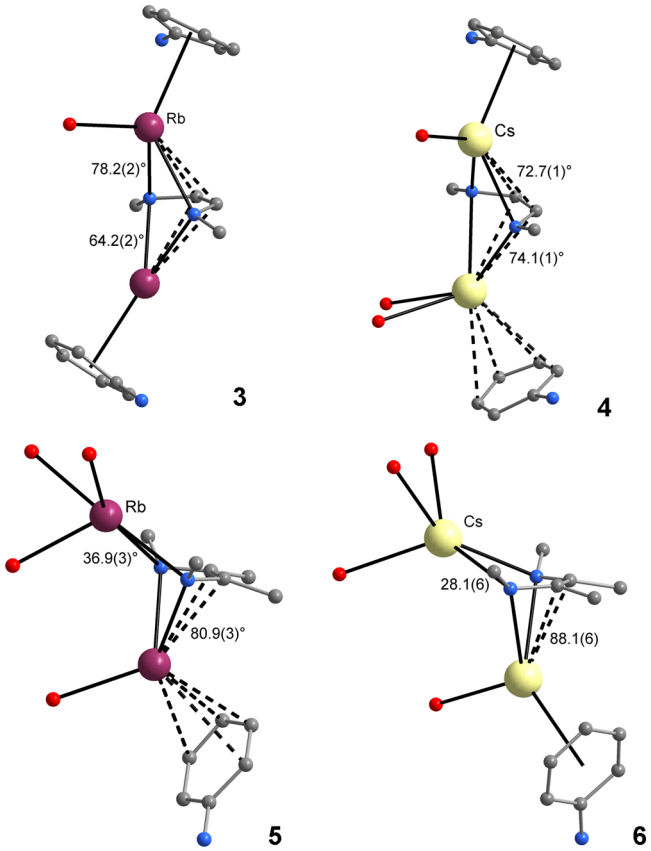

Figure 1. Comparison of the M_2(DAD) structural cores in compounds **3**–**6** showing the displacement angles δ for the metal atoms.

observed displacement angles for the Rb and Cs atoms are relatively large as compared to the Li, Na, and K cases (41–70°), thus arguing for an increased contribution of π-coordination of the DAD backbone in **3** and **4**. In the $(^{Me2}DAD^{Dipp})^{2-}$ complexes **5** and **6**, the M_2(DAD) motif is less symmetric and comprises one metal atom which is situated close to the ligand's C_2N_2 plane, and one metal atom which is attached "side-on" to the enediamide unit (σ,π-coordination, *cf.* structure **F** in Scheme 3). Consequently, the molecular structures of **5** and **6** are similar to those of their lighter homologues. However, the displacement angle of the π-coordinated metal atom is closer to 90° in **5** (81°) and **6** (88°) than in the Li, Na, and K complexes (76–78°),[31] which indicates again a more efficient π-coordination for Rb and Cs. For the σ-coordinated metal atom in the $(^{Me2}DAD^{Dipp})^{2-}$ complexes, no systematic dependency on the metal ionic radius was observed, and the respective δ values for **5** and **6** are in the range observed for the Li, Na, and K derivatives.

A significant structural difference between **3**–**6** and their Li, Na, and K analogues is that the metal atoms are predominantly coordinatively saturated by π-coordinated Dipp substituents rather than σ-coordinated solvent molecules. In **3** and **4**, dual M···Dipp contacts between the $M_2(^{H2}DAD^{Dipp})$ units (best described as η^6 and η^6 for **3**, and η^6 and η^4 for **4**) lead to the formation of ribbon-like polymeric chains (Figure 2). The different degrees of solvation are assumedly supported by the different metal ionic radii of Rb and Cs. In **3**, the spacial conditions allow for additional coordination of only one THF molecule to one of the rubidium atoms (Rb1). In contrast, **4** contains two types of coordinated DME molecules: one is attached to a cesium atom (Cs2) in a typical $\kappa O,\kappa O'$-bidentate mode, and the other one links two symmetry-equivalent Cs atoms (Cs1, Cs1′) of adjacent chains in a $\kappa O/\kappa O'$-bridging mode. The result is a two-dimensional polymeric structure for **4**, which is in agreement with the observed exceedingly low solubility of this compound.

In **5** and **6**, only the π-coordinated metal atom is coordinatively saturated by a Dipp group of an adjacent molecule (**5**: η^4; **6**: η^6), thus forming a polymeric zigzag-chain structure rather than a two-stranded ribbon (Figure 3). Different from **4** and **5**, the degree of solvation is equal in **5**

Table 2. Selected Geometric Parameters of Alkali Metal Enediamide Complexes (δ Angles in °, Interatomic Distances in pm)

M	metal fragment	δ	M–N	M···C	C=C	C–N
			$M_2(^{H2}DAD^{Dipp})$			
Li[29]	σ-Li(DME)	64.1(1)	203.2(2), 209.9(2)	240.5(2), 240.9(2)	136.2(2)	140.5(1)
Na[29]	σ-Na(DME)	49.9(1)	239.2(1), 239.4(1)	289.4(1), 289.8(1)	135.5(2)	140.0(2), 140.5(2)
	σ-Na(diglyme)	70.1(1)	243.2(1), 244.1(2)	269.6(1), 269.7(1)		
K[29]	σ-K(μ-THF)$(THF)_2$	40.6(2)–67.4(2)	255.0(3)–267.3(3)	286.7(3)–321.7(3)	136.7(4)	139.1(4), 141.1(4)
Rb	Rb(η^6-Dipp)	64.2(2)	279.2(1), 288.3(1)	313.3(2), 316.2(2)	136.5(2)	139.8(2), 139.1(2)
	Rb(THF)(η^6-Dipp)	78.2(2)	291.7(1), 295.9(2)	303.6(2), 305.7(2)		
Cs	Cs(κ^1-DME)(η^6-Dipp)	72.7(1)	299.6(2), 304.7(2)	320.3(2), 326.7(2)	137.2(4)	138.0(4), 138.2(3)
	Cs(κ^2-DME)(η^4-Dipp)	74.1(1)	309.4(2), 314.5(2)	329.8(2), 333.2(2)		
			$M_2(^{Me2}DAD^{Dipp})$			
Li[29]	σ-Li(μ-THF)(THF)	23.8(2)	201.9(5), 204.5(4)	279.8(4), 280.8(5)	136.2(3)	141.7(3), 142.0(3)
	π-Li(μ-THF)(THF)	77.6(2)	201.0(5), 203.1(5)	226.0(5), 226.1(5)		
Na[29]	σ-Na$(THF)_2$	38.2(1)	235.4(2), 238.6(2)	304.8(2), 305.8(3)	137.0(3)	140.9(3), 142.0(3)
	π-Na$(THF)_2$	76.6(1)	238.0(2), 238.8(2)	260.8(2), 261.0(2)		
K[29]	σ-K(μ-THF)$(THF)_2$	29.6(2)–30.5(2)	272.5(2)–281.8(2)	348.1(3)–354.9(3)	136.0(4), 136.2(4)	140.8(3)–142.1(4)
	π-K(μ-THF)(η^3-Dipp)	75.7(2)	268.0(2), 276.3(2)	289.9(3), 293.6(3)		
	π-K(μ-THF)(THF)(η^1-Dipp)	72.8(1)	268.6(2), 271.3(2)	295.4(2), 296.0(3)		
Rb	σ-Rb$(THF)_3$	35.4(3)–36.9(3)	286.8(3)–295.1(4)	360.1(4)–363.8(4)	136.2(6)–136.7(6)	140.5(6)–141.4(4)
	π-Rb(THF)(η^4-Dipp)	80.0(3)–80.9(3)	288.6(4)–291.8(4)	302.7(4)–305.7(4)		
Cs	σ-Cs$(THF)_3$	28.1(6)	299.3(4), 304.7(4)	381.3(6), 382.7(6)	133.4(9)	139.7(8), 141.2(7)
	π-Cs(THF)(η^6-Dipp)	88.1(6)	308.2(6), 312.5(5)	310.0(7), 313.4(7)		

https://dx.doi.org/10.1021/acsomega.0c02414
ACS Omega 2020, 5, 19061–19069

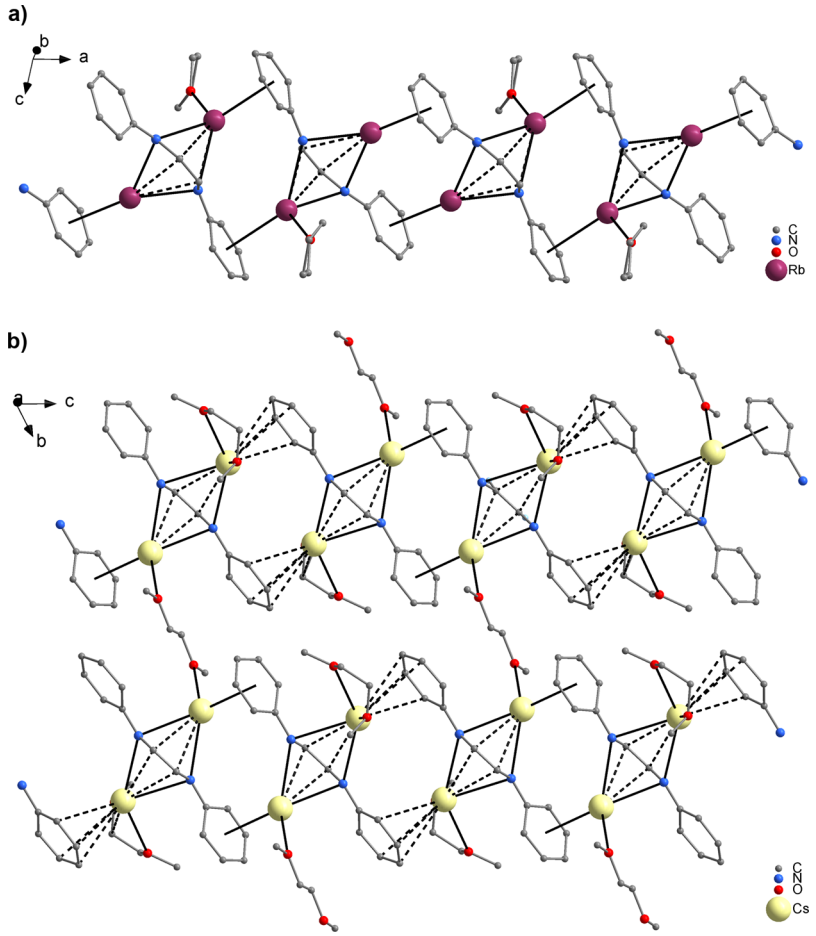

Figure 2. Polymeric ribbon structures of **3** (a) and **4** (b), formed by intermolecular π-Dipp coordination. In **4**, the π-bonded ribbons are further aggregated into a two-dimensional polymer structure by $\kappa O/\kappa O'$-bridging DME ligands. Isopropyl substituents and hydrogen atoms omitted for clarity.

and **6**. In both compounds, the σ-coordinated metal atom is coordinatively saturated by the three THF ligands, and the π-coordinated metal atom has one additional THF ligand. Aggregation of the $M_2(^{Me2}DAD^{Dipp})$ units through intermolecular Dipp-π coordination has been previously observed in the potassium complex, and also, in this case exclusively, the DAD-π-coordinated metal center prefers Dipp groups over solvent THF for coordinative saturation. The Dipp coordination in the related potassium complex is less pronounced than in **5** and **6**, ranging from η^1- to η^3-interactions.[31]

Similar to those observed for the related Li, Na, and K derivatives,[31] the M−N distances in **3**−**6** do not show a significant difference between σ- and π-coordinated metal atoms, while the M···C separations correlate with the respective δ angle (*cf.* Table 2). The C−N and C═C bond lengths within the enediamide unit are virtually identical with those reported for the lighter alkali metal complexes.

CONCLUSIONS

In summarizing the work reported here, we succeeded in the preparation and characterization of the first rubidium and cesium enediamide complexes derived from the sterically demanding 1,4-diaza-1,3-diene ligands 1,4-bis(2,6-diisopropylphenyl)-1,4-diaza-1,3-butadiene (**1**, = $^{H2}DAD^{Dipp}$) and 1,4-bis(2,6-diisopropylphenyl)-2,3-dimethyl-1,4-diaza-1,3-butadiene (**2**, = $^{Me2}DAD^{Dipp}$). Single-crystal X-ray structure determination revealed the presence of similar core structures as known for the related Li, Na, and K complexes. All the alkali metal derivatives of **1** display a σ^2-coordination, while in all complexes derived from **2**, a less symmetric σ,π-coordination was observed. Accordingly, different alkali metal complexes with the same ligand are structurally more similar than complexes of a particular alkali metal with different enediamide ligands, thus confirming the finding observed previously for the Li, Na, and K derivatives.[31] Interestingly, the increased affinity of rubidium and cesium to π-coordination ligands is reflected in the $M_2(DAD)$ core structures only to a small extent, but much more with regard to the coordinative saturation of the metal atoms by *additional* donating moieties. Therefore, the tendency to aggregate through intermolecular π-Dipp coordination, which has been previously seen with the potassium complex $K_2(^{Me2}DAD^{Dipp})(THF)_{3.5}$,[31] is considerably stronger in the rubidium and cesium complexes **3**−**6**. This behavior results in the formation of extended π-coordination polymeric structures and different properties of the rubidium and cesium compounds, such as a significantly reduced solubility.

EXPERIMENTAL SECTION

General Procedures. All operations were performed with the rigorous exclusion of air and moisture under an inert atmosphere of dry argon, employing standard Schlenk, high-vacuum and glovebox techniques (MBraun MBLab; <1 ppm

https://dx.doi.org/10.1021/acsomega.0c02414
ACS Omega 2020, 5, 19061−19069

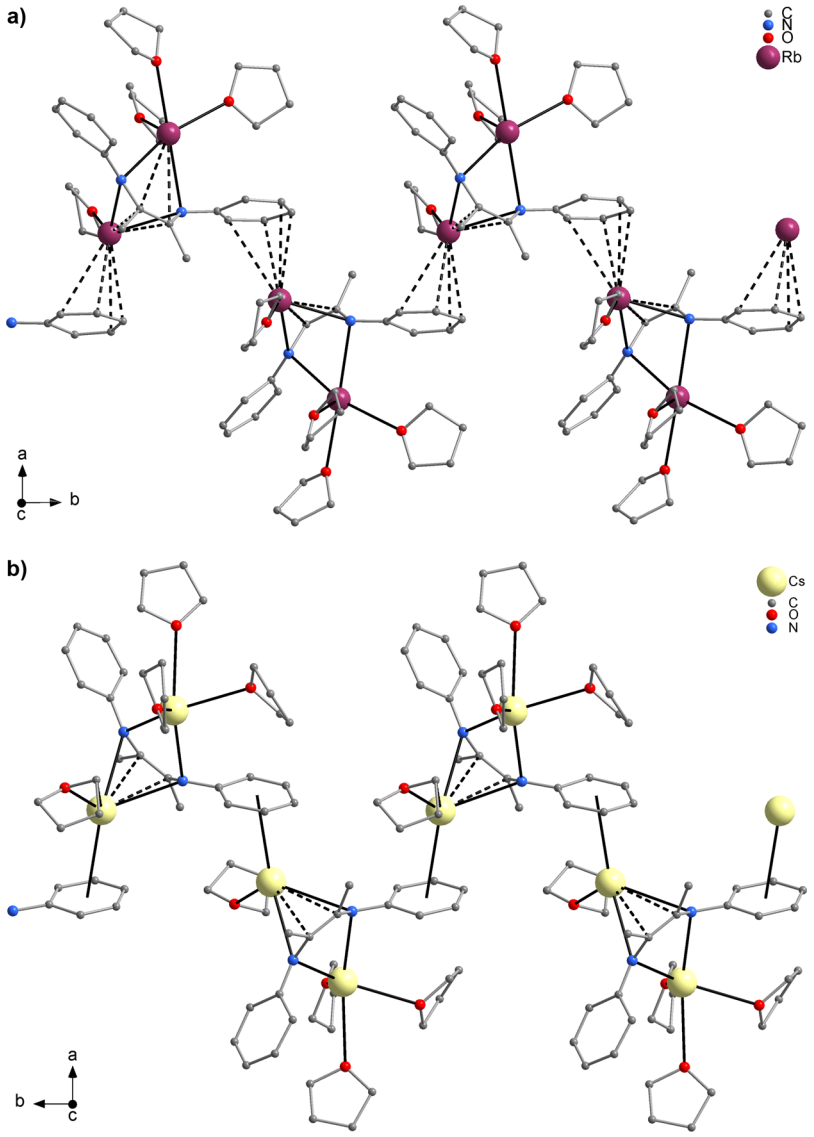

Figure 3. Polymeric zigzag-chain structures of **5** (a) and **6** (b), formed by intermolecular π-Dipp coordination. Isopropyl substituents and hydrogen atoms omitted for clarity.

O_2, <1 ppm H_2O). THF, DME, and toluene were dried over sodium/benzophenone and freshly distilled under a nitrogen atmosphere prior to use. All glassware was oven dried at 120 °C for at least 24 h, assembled while hot, and cooled under vacuum prior to use. The starting materials **1** and **2** were prepared according to literature procedures.[29,30] Metallic rubidium and cesium were purchased from Sigma-Aldrich. **Caution:** Metallic rubidium and cesium are highly reactive and must be stored in a dry box. Utmost care should be exercised when destroying unreacted metal residues. This should be done by a reaction with excess *t*-butanol under nitrogen in order to avoid risk of fire! The NMR spectra were measured in THF-d_8 solutions using Bruker AVANCE III 400 machine (5 mm BBO, ^{1}H: 400.1 MHz; ^{13}C: 100.6 MHz). ^{1}H and ^{13}C shifts are referenced to internal solvent resonances and reported in parts per million relative to tetramethylsilane. IR spectra were measured using an ATR IR spectrometer Bruker Vertex V70. Mass spectra (EI, 70 eV) were run on a MAT 95 apparatus. Raman spectra were measured using a TriVista 777 (S&I, Germany). The excitation laser wavelength was 532 nm, laser power was set to be below 2.5 mW at the samples to avoid decomposition. Only the Stokes side of the Raman spectra was recorded. All spectra were taken at room temperature. The spectral background was removed by applying a Fourier filtering technique. Microanalyses of the title compounds were performed using a VARIO EL cube. For details on the single-crystal X-ray crystallographic studies, see Table 1. The crystal structures reported in this article were solved with SHELXT-2016[36] and refined by full matrix least-squares methods on F^2 using SHELXL-2016.[37]

Synthesis of Rb and Cs Complexes Derived from 1,4-Bis(2,6-diisopropylphenyl)-1,4-diaza-1,3-butadiene (1, = ^{H2}DAD^{Dipp}) and 1,4-Bis(2,6-diisopropylphenyl)-2,3-dimethyl-1,4-diaza-1,3-butadiene (2, = ^{Me2}DAD^{Dipp}) (General Procedure). Specified amounts of **1** or **2** were dissolved in THF or DME and an excess of metallic rubidium or cesium was added. The mixture was stirred at room temperature until the typical color change from yellow (free DAD ligand) over dark red (DAD radical anion) to orange (DAD dianion) had occurred (*ca.* 24 h). Residual metal particles were removed by filtration, and the orange filtrate was concentrated *in vacuo* to a total volume of ca. 20 mL.

https://dx.doi.org/10.1021/acsomega.0c02414
ACS Omega 2020, 5, 19061−19069

Crystallization at 5 °C provided the crystals of the title compounds which were isolated by filtration and briefly dried under vacuum.

*Rb_2(^{H2}DAD^{Dipp})(THF) (**3**).* From Rb metal (0.68 g, 7.96 mmol) and **1** (1.0 g, 2.66 mmol) in 70 mL of THF. Yield of red prisms: 1.32 g (80%). mp 120 °C (dec.). Anal. Calcd for $C_{30}H_{44}N_2ORb_2$ (M_r = 619.63): C, 58.15; H, 7.16; N, 4.52. Found: C, 57.65; H, 6.82; N, 4.66. ^{1}H NMR (400 MHz, THF-d_8, 22 °C): δ 6.49−6.60 (m_{br}, 6H, C*H*-Dipp), 5.48−5.65 (m_{br}, 2H, C*H*-DAD), 3.81 (s_{br}, 4H, $(CH_3)_2CH$Dipp), 3.65 (m, THF), 1.81 (m, THF), 1.09−1.15 (m_{br}, 24H, $(CH_3)_2$CHDipp) ppm. ^{13}C NMR (100 MHz, THF-d_8, 22 °C): δ 155.7 (*C*Dipp), 135.4 (*C*Dipp), 123.0 (*CH*Dipp), 121.8 (*CH*-DAD), 107.8 (*CH*Dipp), 68.2 (THF), 27.7 ($(CH_3)_2$CHDipp), 26.3 (THF), 23.0 ($(CH_3)_2$CHDipp) ppm. MS (EI): *m*/*z* (rel. int.) 603 (100) [M−Me]$^+$, 428 (71) [M−THF−2^{i}Pr−2Me]$^+$, 376 (9) [DAD]$^+$, 333 (71) [DAD−^{i}Pr]$^+$. IR (ATR): ν 2959 m (ν_s CH_{aliph}), 2862 m (ν_{as} CH_{aliph}), 1574 s (ν C═C_{Ring}), 1529 w (ν C═C_{Ring}), 1460 w (δ_{as} CH_{aliph}), 1378 versus (δ_s CH_{aliph}), 1134 m (ν C−N), 1096 versus (ν_{as} C−O−C), 769 m (δ CH_{Ring}), 736 versus (δ CH_{Ring}) cm^{-1}.

*Cs_2(^{H2}DAD^{Dipp})(DME)$_{1.5}$ (**4**).* From Cs metal (1.0 g, 7.52 mmol) and **1** (1.0 g, 2.66 mmol) in 70 mL of DME. Yield of red prisms: 1.85 g (89%). mp 138 °C (dec.). Anal. Calcd for $C_{32}H_{51}Cs_2N_2O_3$ (M_r = 777.59): C, 49.43; H, 6.61; N, 3.60. Found: C, 48.77; H, 6.48; N, 3.82. ^{1}H NMR (400 MHz, pyridine-d_5, 22 °C): δ 6.88−6.94 (m_{br}, 8H, C*H*-Dipp + C*H*-DAD), 3.99−4.13 (m_{br}, 4H, $(CH_3)_2CH$Dipp), 3.48 (s, 4H, DME), 3.26 (s, 6H, DME), 1.32 (d, 24H, ^3J = 6.8 Hz, $(CH_3)_2$CHDipp) ppm. ^{13}C NMR (100 MHz, pyridine-d_5, 22 °C): δ 139.5 (*C*Dipp), 123.4 (*CH*Dipp), 122.9 (*CH*-DAD), 117.6 (*CH*Dipp), 72.0 (DME), 58.6 (DME), 28.2 ($(CH_3)_2$CHDipp), 24.8 ($(CH_3)_2$CHDipp) ppm. MS (EI): *m*/*z* (rel. int.) 406 (4) [CsDAD-2^{i}Pr−Me−2H]$^+$, 378 (20) [DAD + 2H]$^+$, 361 (21) [DAD−Me]$^+$, 333 (86) [DAD−^{i}Pr]$^+$, 162 (100) [Dipp + H]$^+$. IR (ATR): ν 2953 m (ν_s CH_{aliph}), 2861 m (ν_{as} CH_{aliph}), 1576 m (ν C═C_{Ring}), 1523 w (ν C═C_{Ring}), 1451 w (δ_{as} CH_{aliph}), 1387 versus (δ_s CH_{aliph}), 1133 s (ν C−N), 1092 s (ν_{as} C−O−C), 743 m (δ CH_{Ring}), 730 versus (δ CH_{Ring}) cm^{-1}.

*Rb_2(^{Me2}DAD^{Dipp})(THF)$_4$ (**5**)·0.5 THF.* From Rb metal (0.85 g, 10 mmol) and **2** (2.0 g, 4.9 mmol) in 100 mL of THF. Yield of red plates: 3.6 g (81%). mp 240 °C (dec.). Anal. Calcd for $C_{46}H_{76}N_2O_{4.5}Rb_2$ (M_r = 900.04): C, 61.39; H, 8.51; N, 3.11. Found: C, 61.58; H, 8.55; N, 3.21. ^{1}H NMR (400 MHz, THF-d_8, 22 °C): δ 6.61 (d, $^3J_{HH}$ = 7.6 Hz, 4H, C*H*-Dipp), 5.90 (t, 2H, C*H*-Dipp), 3.70 (sep, $^3J_{HH}$ = 6.8 Hz, 4H, $(CH_3)_2CH$Dipp), 3.6 (m, THF), 1.76 (m, THF), 1.62 (s, 6H, DAD-CH_3), 1.21 (d, $^3J_{HH}$ = 6.8 Hz, 12H, $(CH_3)_2$CHDipp), 1.02 (d, $^3J_{HH}$ = 7.2 Hz, 12H, $(CH_3)_2$CHDipp) ppm. ^{13}C NMR (100 MHz, THF-d_8, 22 °C): δ 155.0 (*C*Dipp), 136.4 (*C*Dipp), 123.0 (*CH*Dipp), 121.5 (*C*Me-DAD), 108.2 (*CH*Dipp), 68.2 (THF), 27.4 ($(CH_3)_2$CHDipp), 26.3 (THF), 26.0 ($(CH_3)_2$CHDipp), 24.5 ($(CH_3)_2$CHDipp), 19.1 (DAD-CH_3) ppm. MS (EI): *m*/*z* (rel. int.) 633 (1%) [M$^+$−(H, 2CH_3, C_4H_6, 2THF)], 581 (1%) [M$^+$−(2H, 9CH_3, 2THF)], 420 (1%) [M$^+$−(4C_3H_7, C_4H_6, 3THF)], 406 (89%) [^{Me2}DAD^{Dipp} + 2H], 361 (83%) [^{Me2}DAD^{Dipp}−C_3H_7], 202 (95%) [^{Me2}DAD^{Dipp}−(2CH_3, 4C_3H_7)], 806 (1%), 500 (1%), 391 (2%), 228 (5%), 214 (9%), 204 (100%), 188 (79%), 176 (73%), 173 (68%), 160 (90%). IR (ATR): ν 2953 m (ν_s CH_{aliph}), 2861 m (ν_{as} CH_{aliph}), 1577 m (ν C═C_{Ring}), 1523 m (ν C═C_{Ring}), 1457 m (δ_{as} CH_{aliph}), 1402 versus (δ_s CH_{aliph}), 1133 m (ν C−N), 1097 m (ν_{as} C−O−C), 737 s (δ CH_{Ring}) cm^{-1}.

*Cs_2(^{Me2}DAD^{Dipp})(THF)$_4$ (**6**)·THF.* From Cs metal (1.33 g, 10 mmol) and **2** (2.0 g, 4.9 mmol) in 100 mL of THF, followed by crystallization at 5 °C. Yield of orange plates: 4.06 g (80%). mp 229 °C. Anal. Calcd for $C_{48}H_{80}Cs_2N_2O_5$ (M_r = 1030.97): C, 55.92; H, 7.82; N, 2.72. Found: C, 55.35; H, 7.44; N, 3.00. ^{1}H NMR (400 MHz, THF-d_8, 22 °C): δ 6.61 (d, $^3J_{HH}$ = 7.6 Hz, 4H, C*H*-Dipp), 5.88 (t, 2H, C*H*-Dipp), 3.76 (sep, 4H, $(CH_3)_2CH$Dipp), 3.6 (m, THF), 1.76 (m, THF), 1.56 (s, 6H, DAD-CH_3), 1.17 (d, $^3J_{HH}$ = 6,8 Hz, 12H, $(CH_3)_2$CHDipp), 1.03 (d, $^3J_{HH}$ = 6,0 Hz, 12H, $(CH_3)_2$CHDipp) ppm. ^{13}C NMR (100 MHz, THF-d_8, 22 °C): δ 154.0 (*C*Dipp), 136.0 (*C*Dipp), 123.6 (*CH*Dipp), 121.7 (*C*Me-DAD), 108.1 (*CH*Dipp), 68.2 (THF), 27.2 ($(CH_3)_2$CHDipp), 26.3 (THF), 25.4 ($(CH_3)_2$CHDipp), 24.8 ($(CH_3)_2$CHDipp), 19.6 (DAD-CH_3) ppm. MS (EI): *m*/*z* (rel. int.) 898 (1%) [M$^+$−4CH_3], 806 (93%) [M$^+$−(C_6H_9, THF)], 761 (5%) [M$^+$−(2H, C_6H_9, C_3H_7, THF)], 406 (72%) [^{Me2}DAD^{Dipp} + 2H], 361 (72%) [^{Me2}DAD^{Dipp}−C_3H_7], 202 (98%) [^{Me2}DAD^{Dipp}−(2CH_3, 4C_3H_7)], 1013 (1%), 848 (1%), 666 (1%), 604 (7%), 501 (15%), 417 (8%), 387 (8%), 335 (34%), 313 (6%), 285 (15%), 204 (100%), 188 (46%), 179 (54%), 160 (64%). IR (ATR): ν 2958 s (ν_s CH_{aliph}), 2859 m (ν_{as} CH_{aliph}), 1576 s (ν C═C_{Ring}), 1528 w (ν C═C_{Ring}), 1459 m (δ_{as} CH_{aliph}), 1403 versus (δ_s CH_{aliph}), 1135 m (ν C−N), 1097 m (ν_{as} C−O−C), 744 s (δ CH_{Ring}) cm^{-1}.

■ ASSOCIATED CONTENT

Supporting Information

The Supporting Information is available free of charge at https://pubs.acs.org/doi/10.1021/acsomega.0c02414.

Raman spectra for compounds **3** and **4** and NMR (^{1}H and ^{13}C) and IR spectra of all title compounds (PDF)

Crystallographic data of compounds 3-6 (CIF)

Accession Codes

CCDC 1960467−1960470 contain the supplementary crystallographic data for this paper. These data can be obtained free of charge via www.ccdc.cam.ac.uk/data_request/cif, or by emailing data_request@ccdc.cam.ac.uk, or by contacting the Cambridge Crystallographic Data Centre, 12 Union Road, Cambridge CB2 1EZ, UK; fax: +44 1223 336033.

■ AUTHOR INFORMATION

Corresponding Authors

Rüdiger Goldhahn − *Institut für Physik, Otto-von-Guericke-Universität, Magdeburg, 39106 Magdeburg, Germany*; Email: ruediger.goldhahn@ovgu.de

Frank T. Edelmann − *Chemisches Institut, Otto-von-Guericke-Universität, Magdeburg, 39106 Magdeburg, Germany*; orcid.org/0000-0001-5209-0018; Email: frank.edelmann@ovgu.de

Authors

Ramesh Duraisamy − *Chemisches Institut, Otto-von-Guericke-Universität, Magdeburg, 39106 Magdeburg, Germany*

Phil Liebing − *Chemisches Institut, Otto-von-Guericke-Universität, Magdeburg, 39106 Magdeburg, Germany*; orcid.org/0000-0002-4660-1691

Nicole Harmgarth − *Chemisches Institut, Otto-von-Guericke-Universität, Magdeburg, 39106 Magdeburg, Germany*

Volker Lorenz − *Chemisches Institut, Otto-von-Guericke-Universität, Magdeburg, 39106 Magdeburg, Germany*
Liane Hilfert − *Chemisches Institut, Otto-von-Guericke-Universität, Magdeburg, 39106 Magdeburg, Germany*
Martin Feneberg − *Institut für Physik, Otto-von-Guericke-Universität, Magdeburg, 39106 Magdeburg, Germany*
Felix Engelhardt − *Chemisches Institut, Otto-von-Guericke-Universität, Magdeburg, 39106 Magdeburg, Germany*

Complete contact information is available at: https://pubs.acs.org/10.1021/acsomega.0c02414

Notes

The authors declare no competing financial interest.

■ ACKNOWLEDGMENTS

Financial support by the Otto-von-Guericke-Universität Magdeburg is gratefully acknowledged. M.F. and R.G. thank the DFG (German Research Association) for funding within the framework of Major Research Instrumentation Program no. INST 272/230-1.

■ DEDICATION

Dedicated to Professor Karl-Heinz Thiele on the occasion of his 90th birthday.

■ REFERENCES

(1) van Koten, G.; Vrieze, K. 1,4-Diaza-1,3-butadiene (α-Diimine) Ligands: Their Coordination Modes and the Reactivity of Their Metal Complexes. *Adv. Organomet. Chem.* **1982**, *21*, 151−239.
(2) Stufkens, D. J. Spectroscopy, photophysics and photochemistry of zerovalent transition metal α-diimine complexes. *Coord. Chem. Rev.* **1990**, *104*, 39−112.
(3) van Slageren, J.; Klein, A.; Stufkens, D. J. Resonance Raman spectra of d^6 metal-diimine complexes reflect changes in metal-ligand interaction and character of electronic transition. *Coord. Chem. Rev.* **2001**, *219*−*221*, 937−955.
(4) Raghavan, A.; Venugopal, A. Review: Structurally characterized α-diimine complexes of s-. and p-block elements. *J. Coord. Chem.* **2014**, *67*, 2530−2549.
(5) Haeri, H. H.; Duraisamy, R.; Harmgarth, N.; Liebing, P.; Lorenz, V.; Hinderberger, D.; Edelmann, F. T. *ChemistryOpen* **2018**, *7*, 701−708 and references cited therein.
(6) Scholz, J.; Görls, H.; Schumann, H.; Weimann, R. Reaction of Samarium 1,4-Diaza-1,3-diene Complexes with Ketones: Generation of a New Versatile Tridentate Ligand via 1,3-Dipolar Cycloaddition. *Organometallics* **2001**, *20*, 4394−4402.
(7) Trifonov, A. A. Reactions of ytterbocenes with diimines: steric manipulation of reductive reactivity. *Eur. J. Inorg. Chem.* **2007**, *2007*, 3151−3167.
(8) Makhrova, T. V.; Fukin, G. K.; Cherkasov, A. V.; Trifonov, A. A. Diazadienes in lanthanide chemistry: a new insight into old ligands. Synthesis, structures, and properties of complexes $\{[(R)\text{-}CNC_6H_3Pr^i_2]_2\}Lu(THF)_2(\mu\text{-}Cl)_2Li(THF)_2$ (R = CH_3 or CH_2). *Russ. Chem. Bull.* **2008**, *57*, 2285−2290.
(9) Mahrova, T. V.; Fukin, G. K.; Cherkasov, A. V.; Trifonov, A. A.; Ajellal, N.; Carpentier, J.-F. Yttrium Complexes Supported by Linked Bis(amide) Ligand: Synthesis, Structure, and Catalytic Activity in the Ring-Opening Polymerization of Cyclic Esters. *Inorg. Chem.* **2009**, *48*, 4258−4266.
(10) Panda, T. K.; Pal, K.; Tsurugi, H.; Mashima, K. 1,4-Diaza-1,3-butadiene complexes of lanthanides: syntheses, structures and reactivity. *Kidorui* **2009**, *54*, 202−203.
(11) Panda, T. K.; Kaneko, H.; Pal, K.; Tsurugi, H.; Mashima, K. Salt Metathesis and Direct Reduction Reactions Leading to Group 3 Metal Complexes with a N,N'-Bis(2,6-diisopropylphenyl)-1,4-diaza-1,3-butadiene Ligand and Their Solid-State Structures. *Organometallics* **2010**, *29*, 2610−2615.
(12) Pan, C.-L.; Chen, W.; Song, J. Lanthanide(II)-alkali sandwich complexes with cation-arene π interactions: synthesis, structure, and solvent-mediated redox transformations. *Organometallics* **2011**, *30*, 2252−2260.
(13) Shestakov, B. G.; Makhrova, T. V.; Lyssenko, K. A.; Trifonov, A. A. Diazadienes in lanthanide chemistry: transformation in the diamide and enamine amide ligand systems. Synthesis, structures, and properties of complexes $(2,6\text{-}Pr^i_2C_6H_3N\text{-}C(=CH_2)C(=CH_2)\text{-}NC_6H_3Pr^i_2\text{-}2,6)\text{-}Yb(THF)_2(\mu\text{-}Cl)_2Li(THF)_2$ and $(2,6\text{-}Pr^i_2C_6H_3N\text{-}(H)C(Me)=C(Me)\text{-}NC_6H_3Pr^i_2\text{-}2,6)GdCl(THF)(\mu\text{-}Cl)_2Li(THF)_2$. *Russ. Chem. Bull.* **2013**, *62*, 412−418.
(14) Trifonov, A. A.; Shestakov, B.; Long, J.; Lyssenko, K.; Guari, Y.; Larionova, J. An Organoytterbium(III) Complex Exhibiting Field-Induced Single-Ion-Magnet Behavior. *Inorg. Chem.* **2015**, *54*, 7667−7669.
(15) Klementyeva, S. V.; Petrov, P. A.; Starikova, A. A.; Konchenko, S. N. Erbium Mixed-Ligand β-Diketiminato-Diamido Complex: Unusual Structure of Diamide Ligand. *ChemistrySelect* **2018**, *3*, 1262−1267.
(16) Chamberlain, L. R.; Durfee, L. D.; Fanwick, P. E.; Kobriger, L. M.; Latesky, S. L.; McMullen, A. K.; Steffey, B. D.; Rothwell, I. P.; Foltin, K.; Huffman, J. C. Intramolecular coupling of η^2-iminoacyl and η^2-acyl functions at Group 4 and Group 5 metal centers: structure and spectroscopic properties of the resulting enamidolate and enediamide complexes. *J. Am. Chem. Soc.* **1987**, *109*, 6068−6076.
(17) Durfee, L. D.; McMullen, A. K.; Rothwell, I. P. Intramolecular coupling of η^2-iminoacyl groups at Group 4 metal centers: a kinetic study of the carbon-carbon double-bond-forming reaction. *J. Am. Chem. Soc.* **1988**, *110*, 1463−1467.
(18) Hessen, B.; Bol, J. E.; De Boer, J. L.; Teuben, J. H.; Teuben, J. H. Enediamide complexes of hafnium; X-ray structure of $[(C_5Me_5)\text{-}Hf(Me_2CH)NCHCHN\text{-}(CHMe_2)(\mu\text{-}H)]_2$. *J. Chem. Soc., Chem. Commun.* **1989**, 1276−1277.
(19) Pindado, G. J.; Thornton-Pett, M.; Bochmann, M. New monocyclopentadienyl complexes of Group 4 and 5 metals with chelating nitrogen ligands. Crystal and molecular structures of $[Zr(\eta^3\text{-}C_3H_5)(\eta^4\text{-}Ph_2N_2C_2Me_2\text{-}2,3)Cp'']$ and $[TaCl_2\{\eta^4\text{-}C_6H_4(NSiMe_3\text{-}1,2)_2\}Cp'']$ [Cp" = $C_5H_3(SiMe_3)_2$-1,3]. *J. Chem. Soc., Dalton Trans.* **1998**, 393−400.
(20) Kawaguchi, H.; Yamamoto, Y.; Asaoka, K.; Tatsumi, K. Mono(pentamethylcyclopentadienyl)tantalum Complexes Containing a Structurally Versatile Enediamido(2-) Ligand. *Organometallics* **1998**, *17*, 4380−4386.
(21) Ong, T.-G.; Wood, D.; Yap, G. P. A.; Richeson, D. S. Transformations of Aryl Isocyanide on Guanidinate-Supported Organozirconium Complexes To Yield Terminal Imido, Iminoacyl, and Enediamido Ligands. *Organometallics* **2002**, *21*, 1−3.
(22) Galindo, A.; del Río, D.; Mealli, C.; Ienco, A.; Bo, C. Folded 2,5-diazapent-3-ene metallacycle in ene-diamido group 4 metal compounds: DFT and AIM analyses. *J. Organomet. Chem.* **2004**, *689*, 2847−2852.
(23) De Waele, P.; Jazdzewski, B. A.; Klosin, J.; Murray, R. E.; Theriault, C. N.; Vosejpka, P. C.; Petersen, J. L. Synthesis of Hafnium and Zirconium Imino−Amido Complexes from Bis-imine Ligands. A New Family of Olefin Polymerization Catalysts. *Organometallics* **2007**, *26*, 3896−3899.
(24) Mealli, C.; Ienco, A.; Phillips, A. D.; Galindo, A. A critical review of electronic effects in enediamido and α-diimino complexes of the group 4 metals. *Eur. J. Inorg. Chem.* **2007**, *2007*, 2556−2568.
(25) Thomson, R. K.; Schafer, L. L. Synthesis, Structure, and Insertion Reactivity of Zirconium and Hafnium Amidate Benzyl Complexes. *Organometallics* **2010**, *29*, 3546−3555.
(26) Greulich, S.; Klein, A.; Knödler, A.; Kaim, W. Qualitatively Different Reactivities of Hydride Reagents toward $[(\alpha\text{-diimine})(\eta^5\text{-}C_5Me_5)ClIr]^+$ Cations: Substitution, Electron Transfer (Reduction), or Stepwise Hydrogenation. *Organometallics* **2002**, *21*, 765−769.

(27) Kaim, W.; Sieger, M.; Greulich, S.; Sarkar, B.; Fiedler, J.; Záliš, S. The 1,4-diazabutadiene/1,2-enediamido non-innocent ligand system in the formation of iridaheteroaromatic compounds: Spectroelectrochemistry and electronic structure. *J. Organomet. Chem.* **2010**, *695*, 1052−1058.
(28) Liu, Y.; Li, S.; Yang, X.-J.; Yang, P.; Gao, J.; Xia, Y.; Wu, B. Synthesis and Structure of a Zinc-Zinc-Bonded Compound with a Monoanionic α-Diimine Ligand, [LZn-ZnL] (L = $[(2,6\text{-}^{i}Pr_2C_6H_3)\text{-}NC(Me)]^{2-}$). *Organometallics* **2009**, *28*, 5270−5272.
(29) Jafarpour, L.; Stevens, E. D.; Nolan, S. P. A sterically demanding nucleophilic carbene: 1,3-bis((2,6-diisopropylphenyl)-imidazole-2-ylidene). Thermochemistry and catalytic application in olefin metathesis. *J. Organomet. Chem.* **2000**, *606*, 49−54.
(30) Dieck, H.; Svoboda, M.; Greiser, T. Bis(diazadien)metall(0)-Komplexe, IV. Nickel(0)-bis(chelate) mit aromatischen N-Substituenten/ Bis(diazadiene)metal(O) Complexes, IV. Nickel(0)-bis-(chelates) with Aromatic N-Substituents. *Z. Naturforsch., B: J. Chem. Sci.* **1981**, *36*, 823−832.
(31) Duraisamy, R.; Liebing, P.; Harmgarth, N.; Lorenz, V.; Hilfert, L.; Busse, S.; Engelhardt, F.; Edelmann, F. T. The Manifold Structural Chemistry of Alkali Metal Enediamide Complexes. *Eur. J. Inorg. Chem.* **2019**, *2019*, 3343−3351.
(32) Hathaway, C. E.; Temple, P. A. Raman Spectra of the Alkali Azides: KN_3, RbN_3, CsN_3. *Phys. Rev. B: Solid State* **1971**, *3*, 3497−3503.
(33) Ti, S. S.; Kettle, S. F. A.; Ra, Ø. Weaker Spectral Features in the Raman Spectra of MN_3 (M = K, Rb, Cs). *J. Raman Spectrosc.* **1977**, *6*, 5−12.
(34) Oxford Diffraction. *CrysAlis*; Oxford Diffraction Ltd.: Abingdon, Oxfordshire, England, 2006.
(35) Stoe & Cie. *X-Area and X-Red*; Stoe & Cie: Darmstadt, Germany, 2002.
(36) Sheldrick, G. M. SHELXT - Integrated space-group and crystal-structure determination. *Acta Crystallogr., Sect. A: Found. Adv.* **2015**, *71*, 3−8.
(37) Sheldrick, G. M. Crystal structure refinement with SHELXL. *Acta Crystallogr., Sect. C: Struct. Chem.* **2015**, *71*, 3−8.

https://dx.doi.org/10.1021/acsomega.0c02414
ACS Omega 2020, 5, 19061−19069